Dynamic Stability of a Seaplane in Takeoff

Laurent Dala*

Council for Scientific and Industrial Research, Pretoria 0001, South Africa

This research is based on the investigation into the dynamic stability associated with seaplanes during takeoff. Various forces acting on a hydroplaning hull form have been empirically defined. Such empirical data have shown that, under a certain set of conditions, a hydroplaning hull will begin to porpoise: an instability oscillation in both the vertical direction and about the center of gravity. To investigate the porpoising motion, a shallow water flume was used. It was the first time that such a facility had been used to simulate the dynamic motion of hydroplaning hull forms. An experimental method derived from the store release experiments was derived for the dynamics measurements. The equipment developed led to an analysis of a flat-plate hull porpoising in a supercritical channel. The porpoising limit was then very well defined.

Nomenclature

C_{LB}	=	buoyant lift coefficient
C_{LD}	=	hydrodynamic lift coefficient
C_p	=	position of the center of total pressure forward of the transom
C_v	=	velocity coefficient
d_f	=	fluid depth, m
F_B	=	buoyant force, N
F_n	=	Froude number
h_R	=	fluid pressure head height in reservoir, m
h_{WS}	=	fluid pressure head height in working section, m
L_K	=	wetted length of keel, m
L_{Re}	=	length of characteristics (typically the hull length), m
L_T	=	wetted length of transom, m
p_R	=	static pressure at reservoir, Pa
p_{WS}	=	static pressure at working section, Pa
Re	=	Reynolds number
S	=	surface Area
V	=	displaced volume, m^3
v_B	=	body velocity, m/s
v_f	=	fluid velocity, m/s
v_R	=	fluid velocity in reservoir, m/s
v_W	=	wave velocity, m/s
v_{WS}	=	fluid velocity in working section, m/s
λ_1	=	pressure wetted length-to-beam ratio
ρ	=	density, $\mathrm{kg/m}^3$
τ	=	nominal trim angle, rad
τ_e	=	effective trim angle, rad
τ_p	=	perturbed train angle, rad

I. Introduction

WITH the rising costs of fuel and growing concerns over the environment, seaplanes are becoming interesting alternative forms of transport. But, as described by Stout in [1,2], the hydrodynamic stability prediction is of great importance in the design of seaplanes. Porpoising is a major issue in the design of seaplanes [3–5]. The towing tank is still the main experimental facility used to model the porpoising, as described in [3].

*Professor, R&D Manager, Aeronautic Systems Competency, Meiring Naudé Road, Brumeria; LDala1@csir.co.za;
also Industrial CSIR Chair in Aeronautical Engineering, Department of Mechanical and Aeronautical Engineering, University of Pretoria, Hatfield, Pretoria 0002, South Africa. Member AIAA.

To investigate the dynamic motion of hydroplaning hull forms, a shallow water flume has been modified and used. To perform the experiment, it was necessary to record the motion of the model. At the small scale at which this was performed, weight was crucial; therefore, any recording devices had to be as unobtrusive as possible. It was then decided to adapt the store release tracking system based on video to determine the hull's motion. The effect of mass on the frequency of oscillation was enlightened using the shallow water flume. The general trend showed the frequency of oscillation to decrease as mass increases. The heave and pitch amplitude were also determined in the function of the flow velocity. This research has shown that the vicinity in which sustained porpoising was achieved using a shallow water flume was within the same approximate vicinity as that established in [5].

II. Hydrodynamic Motion

In 1932, Perring and Glauert [4] presented a mathematical approach to study the dynamics of seaplanes experiencing the planing effect. From this work, planing theory has developed. But, one of the most prominent studies into hydroplaning hull forms was performed by Savitsky in [5]. His work resulted in a set of empirical equations being defined that allowed a prismatic planning hull to be designed to a particular performance requirement, and it is still a staple of speedboat design today.

During hydroplaning, there are two forces supporting the weight of the hull: buoyancy and dynamic pressure. With each of these forces, there can be an associated center of pressure. With buoyancy, this is the center of static pressure; and with dynamic forces, this is the center of hydrodynamic pressure. Savitsky, in [5], assumed that, for small angles of attack, the horizontal center of buoyancy was 33% of the wetted length forward of the transom. Assuming that only buoyancy acts on the hull, this would be the point about which no moment due to hydrostatic forces would be applied. It is therefore reasonable to resolve all buoyant forces through this point. Figure 1 reproduces the center of dynamic pressure acts at a point 75% forward of the transom.

As the vessel increases speed, the dominance of forces changes from hydrostatic to hydrodynamic. In [5–7], a formula was derived by taking moments for both hydrostatic and hydrodynamic components about the transom. By dividing through by the total load on the water, the position of the center of total pressure can be found. By studying existing hydroplaning data, a relationship between the position of the center of pressure and the wetted length–to-beam ratio could be established. The resultant equation is shown as follows:

$$C_p = 0.75 - \frac{1}{5.21(C_v^2/l^2) + 2.39} \tag{1}$$

This equation can be represented as a graph for different values of the wetted length-to-beam ratio. This has been described in [5,8]; see Fig. 2.

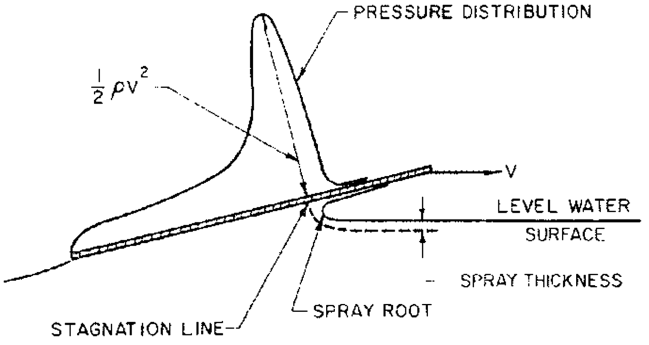

Fig. 1 Pressure distribution on a flat plate [5].

Figure 2 shows that, as the velocity coefficient increases, the center of pressure moves from the center of buoyancy to the center of hydrodynamic pressure, i.e., from 33 to 75%. This does assume, however, a fixed draught and trim angle. In a dynamic environment, both the draught and trim angle can change, resulting in a change in wetted length and lift coefficient.

An instability regime unique to hydroplaning hulls can be experienced under certain conditions. This dynamic instability is known as porpoising. When a hull is porpoising, it is oscillating in both pitch and heave. This can happen even in calm water, and the motion can be neutrally stable, continuing at steady amplitude, or unstable, with the amplitude increasing.

Porpoising can inflict considerable structural damage to a hydroplaning hull. Under extreme conditions, this may result in the hull leaving the water and returning at negative trim angles, causing the hull to submarine, as described in [8,9]. It is therefore important to understand the problem.

Typical research has referred, so far, to a porpoising stability limit: a set of conditions that, once exceeded, will allow a vessel to porpoise. In [9–11], the porpoising phenomenon associated with seaplane floats was investigated. Similar experiments performed in [12,13] showed that the limit of porpoising stability could be written in terms of the velocity coefficient, the lift coefficient, and the trim angle. Work presented in [14–16] consolidated much of the information and developed a set of design tools that allows the porpoising stability of a hull to be estimated by designers. Figure 3 shows their work presented in graphical form.

The lines in the graph represent the porpoising limit for each deadrise angle. If, for a given deadrise angle, the combination of the lift coefficient and trim angle are above the line, then the vessel will

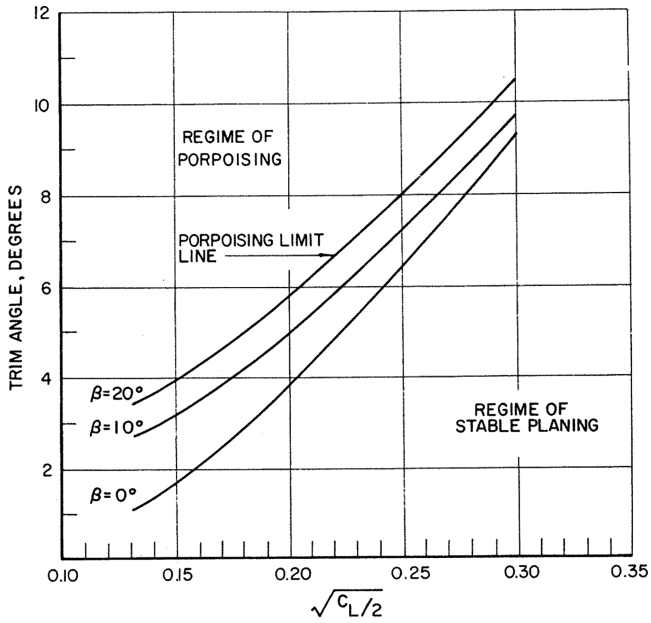

Fig. 3 Porpoising stability limit [14].

tend to porpoise. If a vessel is porpoising, the attitude must be changed such that the trim angle reduces, as described in [5]. Note also that increasing the deadrise angle allows a higher trim angle to be exploited without inducing porpoising characteristics.

In [12–14], numerous experiments were conducted in porpoising and discovered that increasing or decreasing the polar moment of inertia did not change the position or shape of these curves; porpoising still began to exist at the same conditions. The characteristic frequency of the motion does, however, change, with the frequency decreasing with an increase in the polar moment of inertia.

III. Experimental Method

A. Flume Testing

To investigate the forces acting on a hydroplaning hull, an experiment was devised that allows the relationships between various hull forms to be studied. Traditionally, ships and waterborne aircraft have been tested using towing tanks. These tanks are necessarily long, and therefore expensive. They are also few and far between; and

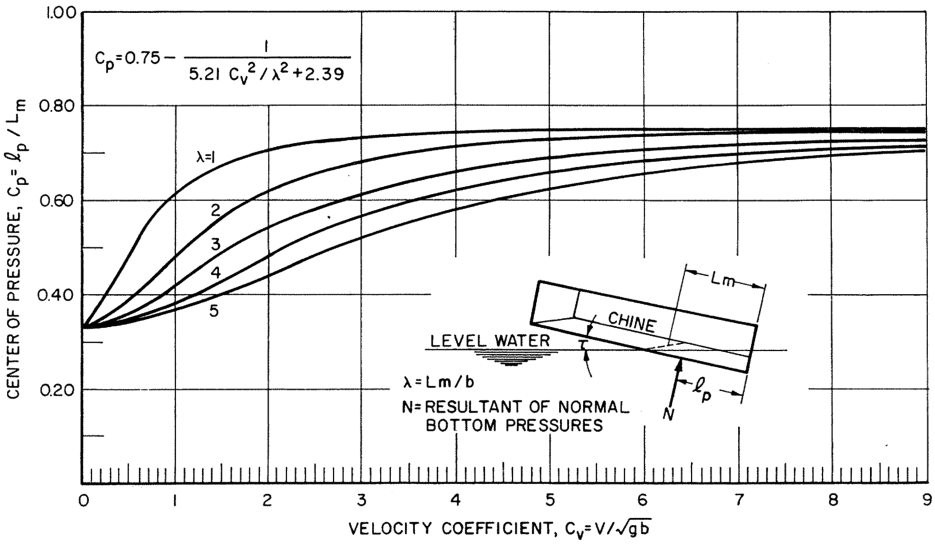

Fig. 2 Center of pressure position against velocity coefficient [5].

Fig. 4 Typical layout of a flume.

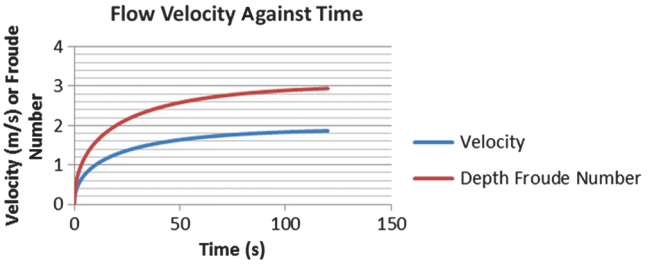

Fig. 5 Froude number and velocity against time for flume working section.

due to their operational nature, there is a limited amount of time available for the collection of data, reduced even further once the settling time for the experiment is allowed for.

By comparison, hydraulic flumes are considerably smaller for the same working cross section, cheaper to construct, and more commonplace. Also, an experiment can be run indefinitely, with the limit being up to the engineer. Drawbacks associated with a flume are the effects of surface wave interference and, more important, the effects that the water energy level has on the wave system inherent with the tests: all of which interfere with results. Figure 4 shows an example of a flume.

One of the differences between a towing tank and a flume is that there is a Froude number associated with the flow of water through an open channel. In the field of hydraulics, this is known as the depth Froude number, and it relates the velocity of wave propagation to the velocity of the water flow, as shown Eq. (2):

$$F_{n_d} = \frac{v_f}{\sqrt{g d_f}} \tag{2}$$

This form of the Froude number can be used to define the flow regime of the fluid. If the depth Froude number exceeds unity, then the flow velocity is greater than the wave propagation velocity, and it is labeled as supercritical. A depth Froude number below unity describes subcritical flow, where wave propagation velocity exceeds the flow velocity. When the fluid flow velocity is equal to the wave propagation velocity, the flow is known as critical. The Froude number at this point is known as the critical Froude number, and it occurs when the fluid is at a depth known as the critical depth.

To model a hydroplaning hull operating above its critical Froude number, the flume had to be capable of achieving supercritical flow. This required the construction of a new working section that allows the fluid Froude number to be controlled. To achieve supercritical flow in a more or less horizontal channel, a pressure head must be maintained upstream of the working section. In the open channel flume, this was done by use of an undershot weir at the start of the working section. A sloped gate enabled the depth of water in the working section, and therefore its velocity and Froude number, to be varied. The dimensions for this working section were dependent on the volume flow rate that the pump was capable of producing. The specification for the working section is shown in Table 1.

This yields a maximum depth Froude number of 2.17.

Table 1 Properties of the flume

Parameter	Value
Volume flow rate Q	0.0124 m^3/s
Working section width w	150 mm
Dam height	260 mm
Minimum depth at Q_{max}	41 mm
Maximum depth at Q_{max}	150 mm
Critical depth	89 mm
Minimum velocity at Q_{max}	0.55 m/s
Maximum velocity at Q_{max}	2.02 m/s
Critical velocity	0.93 m/s

B. Modeling the Flume

With dynamic modeling of the hull form required, it was useful to understand how an accelerating velocity would affect the performance. This requires that the flume be capable of a time-dependent response. To do this, it was necessary to understand the transient period the flume's operation undergoes before a steady-state condition is reached.

1. *Defining the Model*

When the flume was initially switched on, a wave of water proceeded from the inlet, through the working section, and to the outlet. The water level then steadily rose until it reaches the height of the weir. From this point on, the pressure head of the water in the top reservoir increased. Since the weir was set at a particular height, the level only rose upstream of the weir. This in turn caused an increase in velocity downstream of the weir, through the working section. This continued until steady-state equilibrium was reached.

To understand this phenomenon further, Bernoulli's law was applied to the flume, as shown Eq. (3):

$$p_R + \frac{1}{2}\rho v_R^2 + \rho g h_R = p_{\mathrm{WS}} + \frac{1}{2}\rho v_{\mathrm{WS}}^2 + \rho g h_{\mathrm{WS}} \tag{3}$$

There is a volume flow rate associated with the working section. During steady-state operation, this is equivalent to the volume flow rate entering the reservoir. However, during the transient phase, this is not the case. The volume flow rate through the working section can be calculated by applying Bernoulli's equation to obtain the velocity. This velocity can then be applied to the continuity equation to find the volume flow rate.

If the volume flow rate from the pump to the reservoir exceeds that through the working section, this will result in a net increase in volume on the reservoir side. Since the planform area of the reservoir is constant, this manifests itself in an increase in depth.

The flume can be modeled as a quasi-steady state model in the same way as the hull. By assuming that conditions remain constant across a discrete time period, the Bernoulli and continuity laws can be applied. By iterating this across an appropriate time span, the dynamic response of the model can be determined. Figure 5 shows the model as a velocity response to being switched on at full power.

2. *Validating the Model*

To determine whether the model was performing accurately or not, an experiment was performed to validate it. The experiment was to use the same initial conditions as represented in Fig. 5, i.e., switched on at full power. One of the limitations of the flume is its inability to record the instantaneous flow velocity at any point. To avoid problems of comparing the velocities, the experiment focused on comparing the depth in the reservoir section. Since the depth and the velocity are related by Eq. (3), validating the response of the model in terms of depth also validated its response in terms of velocity. A comparison of the model and the experiment is shown in Fig. 6.

Figure 6 shows a very good correlation between experiment and model. There are a few fluctuations in the first few samples. This is believed to be due to the measurement of waves. It was found that, when the flume is first turned on, as it fills, a slight wave reflects off

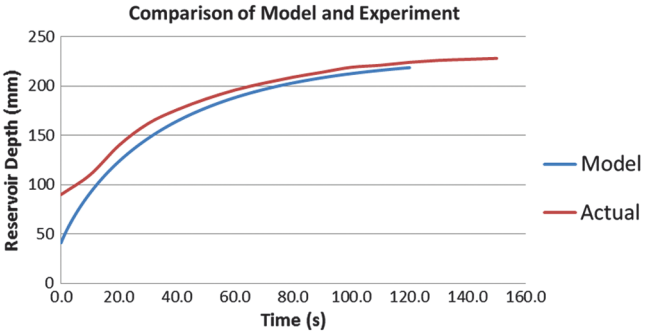

Fig. 6 Comparison between flume model and experimental data.

the working section and oscillates up and down the reservoir. By taking more than one height reading at each interval, an average could have been found, which may have negated this problem.

It can also be seen that there is a slight discrepancy between model and experiment across the whole range. It is believed that part of this is due to the difficulty of judging exactly when the water level reaches the gate; and so, initiating the stopwatch introduces a degree of human error. If the results were modified to eliminate this source of error, the discrepancy between model and experiment would be less.

That being said, the experimental results do show a tendency toward a slightly higher depth than the model does. This could well be due to the fact that friction is not accounted for in the model. Friction would have the effect of causing the fluid velocity to slow a little. Since Bernoulli's theory states a form of conservation of energy, this reduction in velocity would manifest itself in the form of an increase in pressure head, hence the additional depth noted with the experiment.

C. Dynamic Balance

The primary purpose of the experiments is to measure and track the motion of various hull configurations in the flume. In addition to creating the correct conditions in the flume, a method of mounting the model is required. For this, a dynamic balance is necessary.

1. Equipment Requirements

To fill the role effectively, there are a number of requirements the balance must fulfill. The primary purpose of the balance is to allow motion in certain directions while constraining it in others, such as 1) allow motion of the hull in the heave direction, 2) allow motion of the hull in the pitch axis, 3) constrain the hull from motion in the yaw axis, 4) constrain the hull from motion in the transverse direction, 5) constrain the hull from motion in the roll axis, and 6) constrain the hull from fore and aft motion.

In addition to the primary dynamic requirements of the balance, there are those associated with its operation that the balance must be designed to accommodate if the primary requirements are to be met effectively. These are listed here:

1) The weight of the sting must be kept to a minimum to reduce its effect on the model's weight.

2) The balance must have enough adjustment built in to cope with water depths between 40 and 200 mm.

3) The effects of friction in any joints or slides must be minimized.

4) Rotational inertia in any radius arms must be kept to a minimum to avoid its impact on the model's mass.

5) It must be simple to mount alternative hull models to the balance.

2. Balance Design

The balance design is based around a series of sliders. A graphite tube sliding on a steel rod provides the means of locating the model in the vertical axis. To prevent the model yawing, a tail arm with a steel fork locates a second steel slide.

To keep weight down, structural parts were made from balsa wood, since it has very low density and a high resistance to buckling. This allows a lightweight, structural part.

To accommodate motion in the vertical direction, graphite tubes on a steel rod were employed. The steel rod was attached to the base of the balance. Any loads were then transferred from the graphite slides to the base of the balance. The graphite ensured a low-friction contact, whereas the steel ensured structural rigidity, without incurring a weight penalty on the moving parts.

To prevent rotation around the steel rod, a trailing arm was mounted to the balance. This trailing arm had a steel fork mounted to the rear of it, which in turn slid on a second steel rod. This prevented the hull rotating in the yaw direction.

The steel rods were mounted to a laser-cut acrylic base. This base had multiple mounting points on it so that its height above the water could be adjusted. To accommodate motion of the model in pitch, a pivot was mounted to the balance. To reduce friction and weight, the pivot was a very slender plain bearing, of 0.7 mm in diameter. To this pivot was mounted a shoe, which in turn mounted directly to the model.

Figure 7 shows the balance, standing alone on the left; and on the right, it is shown assembled to its carrier frame. The small foot that the hull model mounts to can be seen at the lower extremity of the balance.

D. Hull Model

To get accurate measurements in dynamic motion, the hull has to be lightweight and presents the correct hydrodynamic geometry.

The condition being modeled is for a chines-dry situation. This requires that the water film leave the hull cleanly where the bottom meets the topsides.

These are the two major requirements of the hull form. To maintain a low hull weight, the hull was hotwired from blue foam manually using a jig. The outline was first formed to achieve the correct hydrodynamic shape. Initial testing showed that, although a prismatic hull form is desirable, it would be prudent to design it with a hydrodynamic bow. When the experimental conditions have been reached, this bow is clear of the water and does not interfere with the flow. However, during the startup process as the flume fills, the bow prevents the model from digging in, thus saving both it and the balance from damage. Figure 8 shows the hull mounted to the dynamic balance.

E. Data Acquisition

The experiment method developed for the dynamic measurements of the hull was derived from the store separation free-drop analysis used in wind tunnels, as described in [17].

Free-drop studies are made by realizing or ejecting dynamically scaled store models from a parent aircraft installed in a wind tunnel. The separation characteristics are determined from either a high-

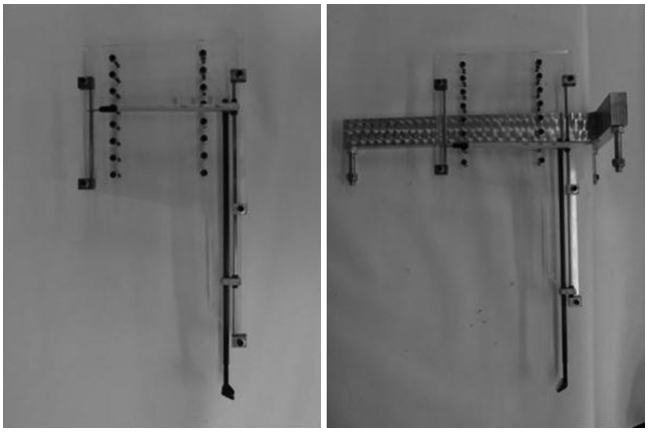

Fig. 7 Dynamic balance.

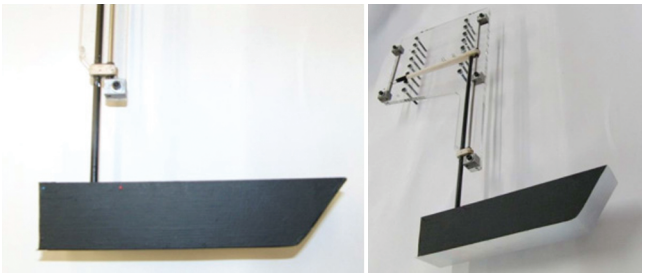

Fig. 8 Hull mounted to the balance.

speed motion camera or multiple-exposure still photographs taken from two or three locations.

The store separation free drop was then adapted to record the dynamic motion of the hull model. At the small scale at which this was performed, the weight of the hull model was crucial; therefore any recording devices had to be as unobtrusive as possible. Video recording offers the least intrusive method of capturing the model's motions, and thus would reduce any errors associated with increasing the mass of the model or interference with its motion due to flying leads or data cables to various other sensors.

There are two basic processes in the use of video capture to provide the required information. The first is to record the actual motion. This is done with a video camera, which produces a series of frames in a set time sequence and provides the raw data used for analysis.

The second part is in analyzing the footage. Since the position of the model can be measured in each frame, it is possible to derive positions with respect to the timeframe of the video, yielding velocities, and from there, accelerations. By combining these two processes, the hull's motion can be tracked.

To record the raw footage, a camera was required. The precision of the test is dependent on two of the camera's parameters. For positional accuracy within each frame, the size of the frame is important. A higher resolution allows a greater positional accuracy to be obtained in each frame.

In addition to the accuracy associated with the two dimensions in each frame, there would be a requirement for accuracy in the time dimension. A higher frame rate allows greater precision in the sampling time step that allows the motion to be tracked more accurately.

Since porpoising is an oscillatory motion, a high frame rate is desirable. If the oscillation were to occur at a rate comparable to the frame rate of the camera, the results may be misleading due to aliasing.

To this end, a machine vision camera was used. The camera is a Blue Cougar S-121C. Its specifics are listed in Table 2.

Figure 9 shows the camera mounted to the tripod at the side of the flume. The working section can also be seen as can the balance's mounting shoe. The black background is to reduce reflections. The angled aluminum plate on the right is the sluice gate. When the experiment is actually running, a black paper shroud is placed all around the flume to reduce reflections.

Table 2 Camera specifications: available sensors

Model name	mvBlueCOUGAR-121
Model variant	G gray/C color
Sensor supplier	Sony
Sensor name	ICX204AL/AQ
Sensor type	Charge-coupled device
Sensor diagonal, mm	6
Indication of lens category to be used	1/3 in.
Resolution of sensor's active area (width × height in [pixels])	1024 × 768
Pixel size (width × height), μm	4.65 × 4.65
Readout type	Progressive
Transfer/shutter type	Full frame
Maximum frame rate, Hz	39
Exposure (step width)	50 μs – 10 s (1 μs)

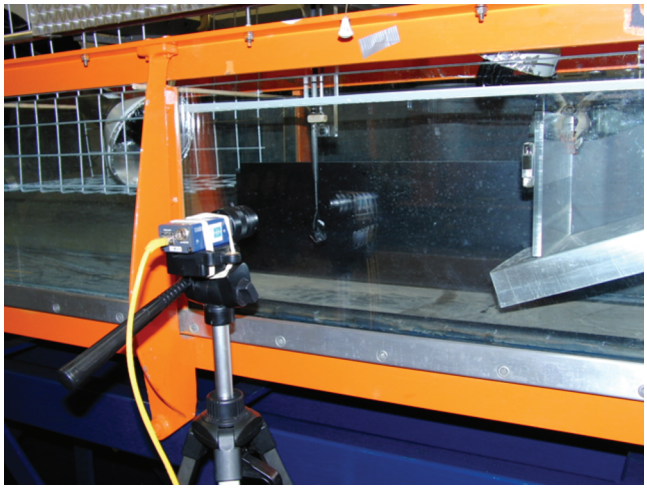

Fig. 9 Experimental layout.

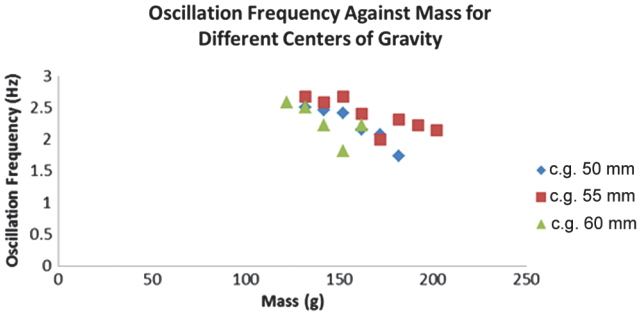

Fig. 10 Oscillation frequency against mass for different centers of gravity.

IV. Experimental Results

After performing the experiment, the video footage was postprocessed using the Simulink model developed. This gives a series of simulations showing the various parameters' oscillations against time for each of these experiments.

A. Effect on Oscillation of Center of Gravity and Mass

Figure 10 shows the effect of mass on the frequency of oscillation. Each dataset represents a different longitudinal center of gravity position, defined in millimeters, from the hull's transom. It can be seen that the general trend shows the frequency of oscillation to decrease as mass increases. It can also be seen that the gradient of this descent is more pronounced the further forward the center of gravity is.

The results for the center of gravity at 50 mm are more uniform than the other two centers of gravity tested, and they have a more defined correlation.

In addition to the frequency, the amplitudes of oscillation in both pitch and heave can be found with respect to the mass. Figure 11 shows the amplitude of pitch oscillation with changing mass at different centers of gravity.

Again, it can be seen that the most uniform and best correlation is obtained when the center of gravity is furthest back. The graph shows that amplitude decreases with increasing mass, and that the effect is more pronounced the further back the center of gravity is. For the furthest forward center of gravity at 60 mm, the graph is almost horizontal, denoting very little change in amplitude with change in mass. Again, the poorest correlation appears to be from the data

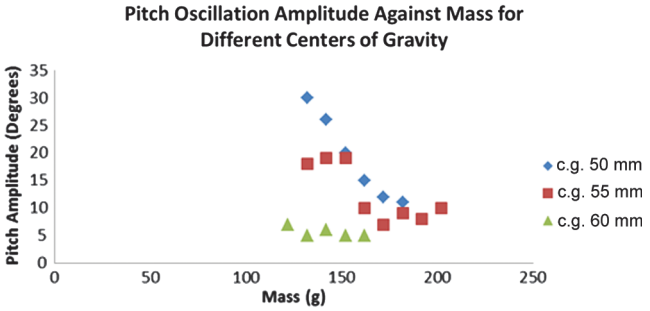

Fig. 11 Pitch oscillation amplitude against mass for different centers of gravity.

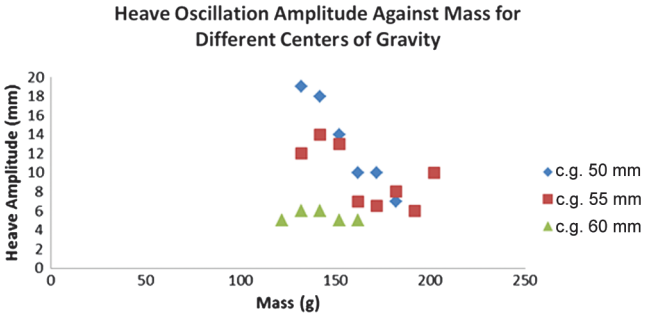

Fig. 12 Heave amplitude against mass for different centers of gravity.

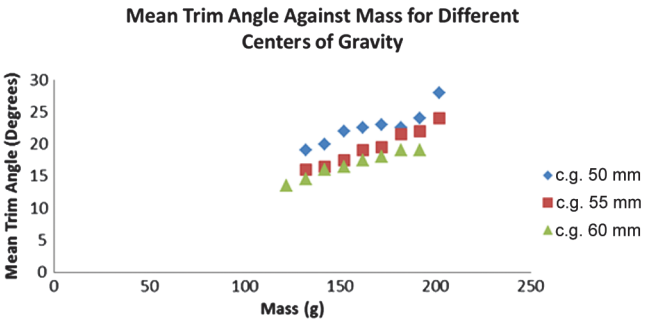

Fig. 13 Mean trim angle against mass for different centers of gravity.

where the center of gravity is at 55 mm. The amplitude of heave motion against mass shows very similar characteristics. Figure 12 shows this.

From Fig. 12, it can be noticed that the best correlation is attained with the center of gravity furthest back. An almost identical relationship with all three datasets is seen with the heave oscillation, which is a decrease in oscillation amplitude with increasing mass. Again, the furthest forward center of gravity shows almost no change in amplitude with change in mass.

The data may also be used to establish the mean trim angle of the hull. This was estimated using the Simulink output graphs. Figure 13 shows how the mean hull trim angle varies with mass.

The graph shows that the trim angle increases with increasing mass. Both centers of gravity at 55 and 60 mm show this to be linear. With the center of gravity at 50 mm, the relationship appears to be linear but drifts a little as the mass increases. The highest mass is then back on the line.

B. Effect on Oscillation of Flow Velocity

Testing the effect of flow velocity was done at a single center of gravity position and mass. Only the velocity was changed. The

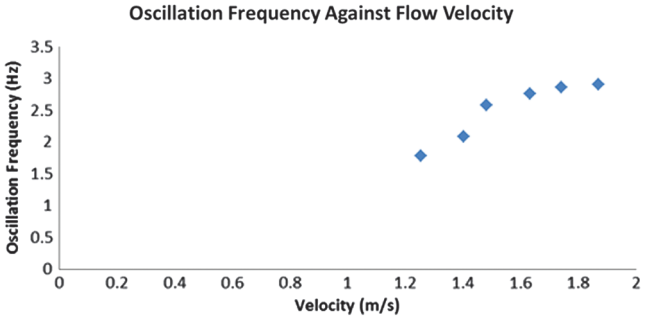

Fig. 14 Oscillation frequency against flow velocity.

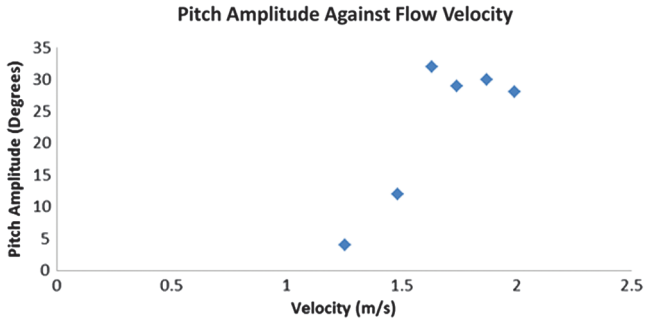

Fig. 15 Pitch oscillation amplitude against flow velocity.

velocities tested are 1.255, 1.402, 1.483, 1.632, 1.741, 1.870, and 1.994 m/s.

Qualitative measurements were made during the experiments. It was found that porpoising was not sustained at very low speeds. There was occasional porpoising that occurred erratically at different periods. But, sustained porpoising was not achieved until the flow reached 1.632 m/s.

When recording the footage, an attempt was made to capture these sporadic moments at low speeds, in order to enable the oscillation to be it analyzed, albeit over a short period.

Figure 14 shows how the frequency of the oscillation changed with the flow speed.

Figure 14 shows that oscillation frequency steadily increases with flow velocity. It should be noted that the first two data points are at velocities of 1.255 and 1.483 m/s. Oscillation during these periods was not sustained; however, when it did occur, the data for these points were recorded. No oscillation was found at 1.402 m/s. There is a slight step jump in the frequency after this point, implying a difference in the mechanics of the oscillation. The last four points are more uniform in this period, again showing the steady increase in the frequency of the oscillation.

Further evidence of the difference between sustained and unsustained oscillations can be seen in Fig. 15. The graph shows how the amplitude of the pitch oscillation varies with flow velocity.

In this instance, there is again a step jump between the points of sustained oscillation and unsustained oscillation. However, this time the jump is far greater. The first two points are of a very different magnitude of amplitude. Once the velocity reaches 1.632 m/s, a relationship can be seen. The amplitude of pitch oscillation steadily decreases with an increase in velocity.

A similar trend is repeated in Fig. 16, showing the amplitude of heave oscillation.

It can be noticed in Fig. 16 that a large step jump is seen in amplitude, corresponding to the point where sustained porpoising was observed. The only noticeable difference is that the decrease in amplitude with an increase in velocity is less pronounced: only being noticeable in the last three points. Figure 17 shows how the mean trim angle varies with velocity.

The trim angle decreases dramatically with increase in velocity. There is apparently a change in gradient at the point where sustained porpoising was observed.

V. Analysis

When looking at the experiment where velocity was changed, it was noted that the oscillation was not sustained at lower speeds. There were, however, periods where the oscillation did exist for short periods. It is believed that the oscillation was triggered by fluctuations in the flow.

It is believed that, if completely smooth flow was achieved, the oscillation may not have taken place at all. Referring back to Figs. 15 and 16, the amplitude of both pitch and heave oscillations was found to vary considerably dependent on whether porpoising was observed to be sustained or not. This can actually be used to define the existence of the phenomenon.

Figure 18 shows pitch amplitude against velocity, with a bounded region added. This region defines the area where sustained porpoising exists at the lowest velocity: in effect, where the phenomenon begins.

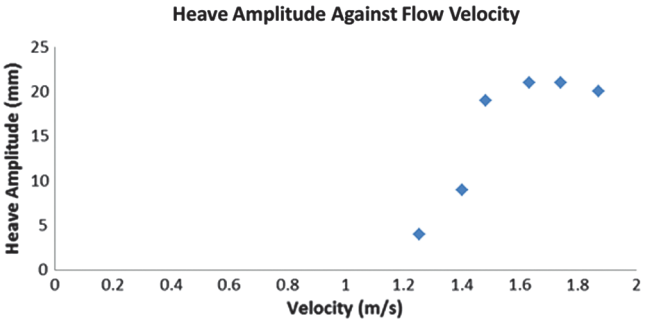

Fig. 16 Heave oscillation amplitude against velocity.

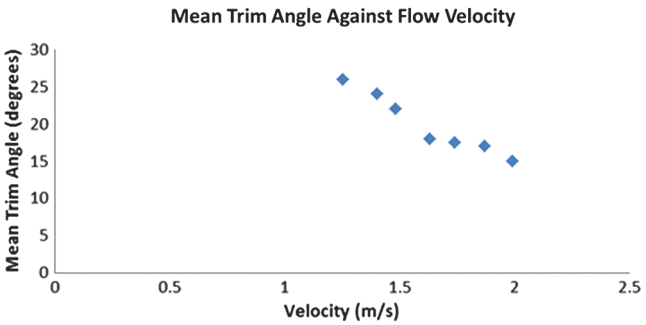

Fig. 17 Mean trim angle against flow velocity.

Table 3 Values of trim angle and $\sqrt{C_L/2}$ for points bounding the porpoising limit

Velocity, m/s	$\sqrt{C_L/2}$	Trim angle, deg
1.483	0.3972122	22
1.632	0.3609471	18

This complies with Savitsky's theory, in [5], of the porpoising limit. To attempt to quantify this theory, a comparison of the data can be plotted. Figure 3 shows the porpoising stability limit, as shown in [5–7].

To make a comparison between the data provided in Fig. 3 and experimental data, the results must be manipulated into the same form as that shown in [5–7]. The average trim angle was measured in degrees, so this already matches. However, other data taken from the test conditions must be given in terms of the lift coefficient.

The lift coefficient can be obtained from the load on the water or the hull's weight. This is given by Eq. (4):

$$C_L = \frac{\Delta}{(1/2)\rho V^2 b^2} \tag{4}$$

By substituting the test values at velocities of 1.483 and 1.632 m/s, it is possible to find the lift coefficient, and hence the $\sqrt{C_L/2}$ value shown on Savitsky's graph [5]. The resultant values are shown in Table 3.

The tests were all performed on flat-bottomed hulls, meaning deadrise was 0 deg. By extracting data from Fig. 3, a comparison between Savitsky data [5] and the data in Table 3 was carried out. It is also necessary to extrapolate Savitsky's data so that it reaches high enough trim angles and lift coefficients. The first comparison show that the vicinity in which sustained porpoising was achieved in the experiment is within the same approximate vicinity as that established in [5]. However, there are still a number of discrepancies. The line between the two experimental points appears to be at a similar gradient to that extrapolated from Savitsky's data. This is unusual, as the points represent a value that, if correct, would be one either side of this line. Being nearly parallel makes this possibility difficult to achieve.

The gradient of the line between the two points is slightly steeper than Savitsky's [5]. This means that, even if the points were to fall either side, it would leave the nonoscillating position in the realm of porpoising and the oscillating position in that of nonporpoising. One possibility is that, at the higher trim angles and lift coefficients at which the experiment takes place, Savitsky's data are no longer applicable. It might be that the porpoising stability limit line gradient has a tendency to increase at higher values. Figure 19 shows a

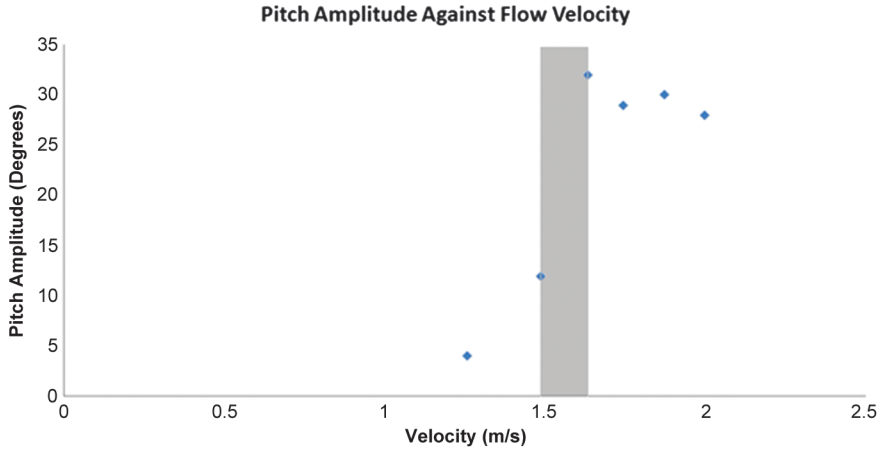

Fig. 18 Region where sustained porpoising occurs for the first time.

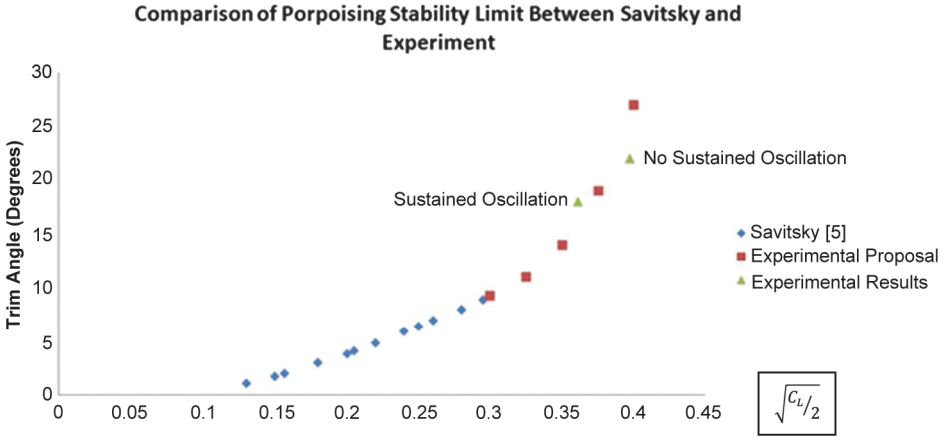

Fig. 19 Data comparison showing porpoising stability limit.

comparison of porpoising stability after corrections between Savitsky's predictions and the experimental data.

VI. Conclusions

The dynamic motion of hydroplaning hull forms has been experimentally tested using a shallow water flume for the first time. The equipment and the experimental method developed for this research have led to an analysis of a hull porpoising in a supercritical channel. From the experimental point of view, this enables a number of conclusions to be drawn.

1) The porpoising motion can be captured using an experimental method derived from the store separation free drop.

2) The porpoising limit is a well-defined region, where unsustained oscillation turns into sustained oscillation.

3) Porpoising motion approximates a sinusoidal curve.

4) Acceleration vertically in heave is greater upward than downward.

But, the main conclusion is that porpoising of a hull can be instigated using a shallow flume with supercritical flow. The experimental method developed from the store separation free drop must still be improved, especially if the video capture presents numerous problems when recording through a glass window in a wet environment as splashes distort the footage, but this can be overcome.

References

[1] Stout, E. G., "Experimental Determination of Hydrodynamic Stability," *Journal of the Aeronautical Sciences*, Vol. 7, No. 2, 1940, pp. 55–61. doi:10.2514/8.10479

[2] Stout, E. G., "Development of High-Speed Water-Based Aircraft," *Journal of the Aeronautical Sciences*, Vol. 17, No. 8, 1950, pp. 457–480. doi:10.2514/8.1698

[3] Van Dyck, R., "Seaplanes and the Towing Tank," *Advanced Marine Vehicles Conference*, AIAA Paper 1989-1533, 1989. doi:10.2514/6.1989-1533

[4] Perring, W. G. A., and Glauert, H., "Stability on the Water of a Seaplane in the Planing Condition," Aeronautical Research Committee, Reports and Memoranda 1493, 1932.

[5] Savitsky, D., "Hydrodynamic Design of Planing Hulls," *Marine Technology*, Vol. 1, No. 1, Oct. 1964, pp. 71–95.

[6] Savitsky, D., and Ward, D., "Procedures for Hydrodynamic Evaluation of Planing Hulls in Smooth and Rough Water," *Marine Technology*, Vol. 13, No. 4, Oct. 1976, pp. 381–400.

[7] Savitsky, D., and Ross, E., "Turbulent Stimulation in the Boundary Layer of Planing Surfaces," Stevens Inst. of Technology, Davidson Lab. Rept. 44, Hoboken, NJ, 1952.

[8] Martin, M., "Theoretical Determination of Motion of High-Speed Planing Craft in Waves," David W. Taylor Naval Ship Research and Development Center Rept. 76-0069, Potomac, MD, April 1976.

[9] Schroder, P., "The Take-Off of Seaplanes, Based on a New Hydrodynamic Reduction Theory," NACA TM-621, May 1931.

[10] Sottorf, W., "Experiments with Planing Surfaces," NACA TM-661, 1932.

[11] Sottorf, W., "Systematic Model Researches on the Stability Limits of the DVL Series of Float Designs," NACA TM-1254, 1949.

[12] Locke, F. W. S., "General Porpoising Tests of Flying Boat Hull Models," NACA-WR-W-96 Advanced Restricted Rept. 3117, 1943.

[13] Davidson, K. S. M., and Locke, F. W. S. Jr, "Some Analyses of Systematic Experiments on the Resistance and Porpoising Characteristics of Flying-Boat Hulls," NACA Advanced Restricted Rept. 3I06, Sept. 1943.

[14] Day, J. P., and Haag, R. J., "Planing Boat Porpoising," Ph.D. Dissertation, Inst. of Naval Architecture, London, 1952.

[15] Payne, P. R., "Coupled Pitch and Heave Porpoising Instability in Hydrodynamic Planing," *Journal of Hydronautics*, Vol. 8, No. 2, April 1974, pp. 58–71. doi:10.2514/3.62979

[16] Payne, P. R., "Errata-Coupled Pitch and Heave Porpoising Instability in Hydrodynamic Planing," *Journal of Hydronautics*, Vol. 9, No. 3, 1975, pp. 127–128. doi:10.2514/3.63032

[17] Arnold, R. J., and Epstein, C. S., "Store Separation Flight Testing," AGARD Flight Test Techniques Series, Vol. 5, AGARD AG-300, April 1986.